J. Fluid Mech. (1968), *vol.* 32, *part* 3, *pp.* 465–488
Printed in Great Britain

A linear model of the Antarctic circumpolar current

By A. E. GILL

Department of Applied Mathematics and Theoretical Physics,
University of Cambridge

(Received 20 July 1967)

A simple frictional wind-driven model of the Antarctic circumpolar current is examined. The geometry includes what are thought to be the main features effecting the current, namely a gap corresponding to Drake Passage and a partial barrier corresponding to the South American peninsula. Solutions obtained by both numerical and analytical methods are presented. The analytic solution, valid for small values of a friction parameter, enables the total rate of transport of water by the current to be calculated as a function of the friction parameter and the wind stress distribution. The width which controls the rate of transport by the current tends to be the narrowest encountered rather than the average width as assumed in earlier zonal models. However, the current spreads out to several times this width due to frictional effects. The values of the eddy viscosity required to give a rate of transport of the observed order are about 10^3 cm^2/s for a bottom-friction model and of the order of 10^8 cm^2/s for a lateral friction model.

1. Introduction

The Southern Ocean, or Antarctic Ocean, occupies a large percentage of the zonal strip of the earth's surface between the fortieth and seventieth parallels (south). Besides being an important water mass in itself, the Southern Ocean serves as a connecting link between the other major oceans. Its most obvious dynamic feature is the strong eastward circumpolar current, an interesting descriptive article on which has recently been written by Kort (1962). The current extends northwards to about 40° S, which is the reason for choosing that parallel as the northern limit of the Southern Ocean. Estimates of the total transport of water by the current vary widely since they depend on the choice of a 'reference level'. Kort, for instance, estimates the total transport as 150 million cubic metres per second. Gordon (1967) made use of a water mass analysis to estimate reference levels in Drake Passage and on that basis obtained a total transport of 220 million cubic metres per second.

Theoretical models of the circumpolar current have been reviewed by Crease (1964) and summarized more recently by McKee (1966). The earlier models were zonally symmetric, the Southern Ocean being treated as a broad channel bounded by two parallels of latitude about 25° apart. The currents were driven by a wind stress at the surface and opposed by some form of frictional stress. However, for generally accepted values of the friction parameters, the transports predicted by these models were far in excess of those observed, indicating a gross over-simplification somewhere in such models. Stommel (1957) suggested that the

geometry of these models was chiefly to blame and pointed out that in closed basins, the currents are essentially frictionless and determined by the Sverdrup (1947) theory, except in narrow boundary layers. For these frictionless currents to exist, meridional barriers must cross each circle of latitude. Stommel drew

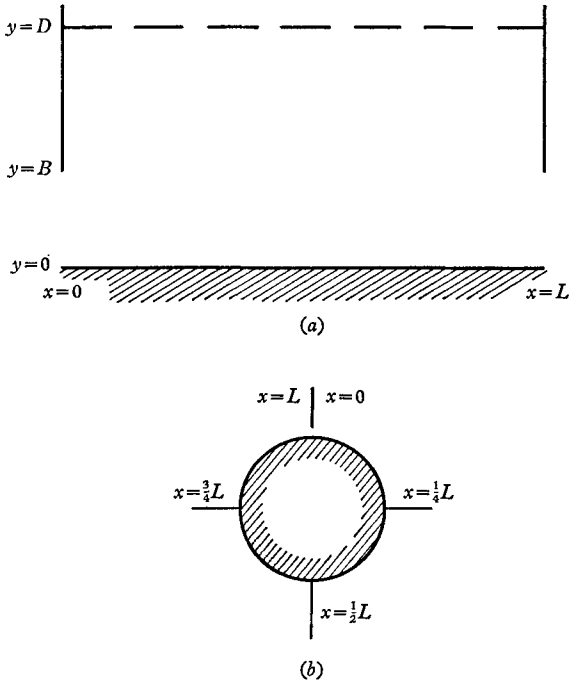

FIGURE 1. The geometry of the model. (*a*) Mercator projection (N–S scale exaggerated). (*b*) Polar projection.

attention to the fact that the South American peninsula and Graham Land (Palmer Peninsula) form meridional barriers which span all but about 5° of latitude, and the island arc to the east partly spans the remaining 5°. He therefore suggested the possibility that 'the current is essentially frictionless except in a narrow region just after it passes through Drake Passage'. Wyrtki (1960) made some calculations based on the Sverdrup theory, but this breaks down at latitudes for which there are no meridional barriers. Stommel (1962) later examined a model where this difficulty was overcome by treating Drake Passage as a porous section in a meridional wall.

In this paper it is proposed to examine the effects of a partial meridional barrier with a gap corresponding to Drake Passage. The geometry chosen for this study is shown in figure 1 and is about the simplest that can include the above features. x, y are co-ordinates measuring distance eastwards and northwards respectively so that L represents the distance around a circle of latitude and B the width of the passage. The origin corresponds to a point at the southern end of Drake Passage, and the line $y = 0$ can be thought of as a crude approximation to the Antarctic coastline. The lines $x = 0$ and $x = L$ represent the same meridian, as is shown by the polar projection, the section $y > B$ being a solid

barrier akin to the South American peninsula. A boundary may be introduced at $y = D$ if desired. Then the model ocean becomes a zonal channel in the limiting case $B = D$ and a closed basin in the other extreme $B = 0$. Thus for $0 < B < D$ the model ocean can be regarded as having a geometry intermediate between these two limiting cases. Stommel, in 1957, suggested a geometry something like that of figure 1 and gave a qualitative idea of how he expected the currents to be distributed, but did not work out details. Here the details will be worked out for a simple dynamical model. The main concern is to understand effects of the *geometry* so that many other effects such as bottom topography (considered by Kamenkovich 1962), thermohaline effects (see Duncan 1966) and the effect of peripheral discharge from Antarctica (see Barcilon 1966, 1967) will not be included in the basic model, although effects of bottom topography will be discussed in §6.

The main effort is directed at solving the problem for a bottom friction model. The relevant dynamical equations are set out in §2 and the parameters of the model discussed. In §3 a picture of the structure of the solution is built up, this being shown in figure 2. Some numerical solutions obtained by Dr J. W. Elder are presented in §4. These are supplemented by an appropriate analytical solution found in §5. The latter solution enables the total transport of water by the current to be estimated for any zonal wind stress distribution and any sufficiently small value of a friction parameter, some results being depicted in figure 6. These results form a basis for a comparison with observations in §6. Effects of (*a*) non-zonality of the wind stress, (*b*) the barrier formed by New Zealand and the shallow water to the south, and (*c*) large-scale bottom topography are discussed. The form of the analytic solution for a lateral friction model is also deduced in §6 and a discussion made as to which form of friction is most realistic.

2. The model, equations and boundary conditions

Dynamically the model is essentially that used by Stommel (1948). The ocean is assumed to be of constant depth, H, and the horizontal momentum equations, representing a balance between the horizontal pressure gradient, the Coriolis force and the friction stress, are integrated over this depth. A rectangular co-ordinate system is used with x, y, z measuring distances eastwards, northwards and upwards respectively. An approximation is of course involved in using such a system but this is not significant when the crude nature of the model is considered. If u, v are the eastward and northward velocity components and ρ the density, the integrated equations involve the mass transport components

$$U = \int_0^H \rho u \, dz, \quad V = \int_0^H \rho v \, dz,$$

and the integral of the pressure p, namely

$$P = \int_0^H p \, dz.$$

The integrated equations have the form

$$\left.\begin{aligned} -fV &= -P_x + X_{\text{surface}} - X_{\text{bottom}}, \\ fU &= -P_y + Y_{\text{surface}} - Y_{\text{bottom}}, \end{aligned}\right\} \tag{2.1}$$

where $f = 2\Omega \sin\theta$ is the Coriolis parameter, Ω being the angular velocity of the earth and θ the latitude. X, Y are the components of stress exerted on the surface by the wind and on the ocean bottom due to friction. Lateral friction has been ignored so that the equations, apart from the inclusion of bottom friction, are those used by Sverdrup (1947, equation (9)). The necessity of a frictional term at latitudes for which there is no meriodinal barrier is immediately seen when the first of (2.1) is integrated along a circle of latitude. This gives

$$\int_0^L X_{\text{surface}}\, dx = \int_0^L X_{\text{bottom}}\, dx, \tag{2.2}$$

that is, the surface force on a narrow zonal strip is balanced by the frictional force on the bottom. In contrast, at latitudes where meridional barriers do exist, the surface force can be balanced by a pressure difference and so friction forces do not necessarily play an important role.

Following Stommel, a linear friction law is assumed so that the equations become

$$\left.\begin{aligned} -fV + rU &= -P_x + X_{\text{surface}}, \\ fU + rV &= -P_y + Y_{\text{surface}}, \end{aligned}\right\} \tag{2.3}$$

with r a constant. This is a valid first approximation for laboratory models in which there is laminar flow, the Ekman layers are thin compared with the depth H of the fluid, and X_y/X is small compared with β/f. Then

$$r = (\nu|f|/2H^2)^{\frac{1}{2}}, \tag{2.4}$$

where ν is the kinematic viscosity of the fluid. Equation (2.4) is often used in more general circumstances to define an eddy viscosity ν corresponding to a given value of r.

In addition to the dynamic equations (2.3) there is the continuity requirement, which implies the existence of a transport function Ψ such that

$$U = -\Psi_y, \quad V = \Psi_x. \tag{2.5}$$

Substitution in (2.3) and elimination of P leads to (cf. Stommel 1948, equation (9))

$$r(\Psi_{xx} + \Psi_{yy}) + \beta\Psi_x = Y_x - X_y, \tag{2.6}$$

where $\beta = df/dy = (2\Omega/R)\cos\theta$, R being the radius of the earth, and can be treated as a constant since the latitudinal scale is assumed small compared with R. The subscript 'surface' has been dropped so X, Y represent components of the surface wind stress.

The boundary conditions are that there be no flux across solid boundaries, that is, that Ψ be constant on solid boundaries. The value of the constant can be set to zero on the boundaries $x = 0$ and $x = L$ but Ψ will have a different value on $y = 0$. This value is a measure of the total transport through the gap and so will be designated Ψ_{tot}. Equation (2.6) together with these boundary conditions is not enough, however, to give a unique solution as some information has been lost in eliminating the pressure. The lost condition is the continuity of pressure along a closed path which circumscribes the pole. Choosing a circle of latitude

for the path, the lost condition is given by (2.2), which, with the aid of (2.3), may be written in the form

$$\int_0^L r\Psi_y dx + \int_0^L X dx = 0, \tag{2.7}$$

the integration being along a path $y =$ constant where $0 < y < B$. This condition was noted in a more general form by Kamenkovich (1961).

There are several parameters needed to describe the system most of which can be regarded as the ratios of length scales. The geometry involves three lengths B, L and D while the governing equation introduces a fourth

$$W = r/\beta. \tag{2.8}$$

This length, which depends on the friction coefficient, is a measure of the width of the western boundary current found in Stommel's solution for a closed basin. Choosing B as the standard length, the three parameters corresponding to these four lengths may be defined as

$$\left.\begin{aligned} \ell &= L/B, \\ d &= B/D, \\ \text{and} \quad \delta &= W/B = r/\beta B. \end{aligned}\right\} \tag{2.9}$$

In addition other parameters may be required to describe the wind stress field, for instance, if this has the form

$$X = T\sin(Ky+\alpha), \quad Y = 0, \tag{2.10}$$

two parameters are involved, namely the wave-number parameter

$$k = KB \tag{2.11}$$

and the phase angle α. The constant T gives the wind stress scale which sets the scale for the transport function but gives rise to no further parameters since the problem is linear.

The appropriate value of the standard length B is not obvious because of the complicated coastline shapes and bathymetry of the area around Drake Passage. In this paper, shallow water regions will be treated as belonging to the land area so that the latitude $y = B$ of the southern tip of South America will be taken as that of Diego Ramirez Island, that is about 56·6° S. The latitude $y = 0$ of the northern tip of the peninsula opposite will be taken as that of Elephant Island, that is about 61·0° S. This makes B about 500 km and ℓ about 42.

Using B as a standard length the equations and boundary conditions can be put in non-dimensional form. Non-dimensional co-ordinates $(\hat{x}, \hat{y})$, stress components $(\hat{X}, \hat{Y})$ and stream function ψ will be defined as follows:

$$(x, y) = B(\hat{x}, \hat{y}), \quad (X, Y) = T(\hat{X}, \hat{Y}), \quad \Psi = T\psi/\beta. \tag{2.12}$$

Then, dropping circumflexes, the equation becomes

$$\delta(\psi_{xx}+\psi_{yy})+\psi_x = Y_x - X_y, \tag{2.13}$$

and the condition (2.7) becomes

$$\delta\int_0^\ell \psi_y dx + \int_0^\ell X dx = 0 \quad \text{for} \quad 0 < y = \text{constant} < 1. \tag{2.14}$$

The boundary conditions are

$$\left.\begin{aligned} &\psi = 0 \quad \text{on} \quad x = 0, \ell \quad \text{for} \quad y > 1, \\ &\psi = \psi_{\text{tot}} \quad \text{on} \quad y = 0, \\ &\psi \text{ is periodic in } x \text{ with period } \ell \quad \text{for} \quad 0 < y < 1. \end{aligned}\right\} \tag{2.15}$$

The boundary condition on $y = d$ will be discussed later. If it is regarded as a solid boundary, then the appropriate condition is

$$\psi = 0 \quad \text{on} \quad y = d. \tag{2.16}$$

3. Structure of the solution for small friction

In this section, the behaviour of the solution as the friction parameter δ tends to zero will be discussed. Knowledge of this behaviour will be exploited in later sections. It will not necessarily be assumed that the product

$$\epsilon = \delta\ell = rL/\beta B^2 \tag{3.1}$$

also approaches zero in view of the large values of the aspect ratio which are of interest. Discussion will be limited to the case in which the wind stress is given by

$$X = X(y), \quad T = 0.$$

Note that the governing equation (2.13) is of the same form as found in certain forced convection problems (Goldstein 1938), so that the discussion below could as well be carried out in terms of an analogue system.

It is convenient to discuss the regions $y > 1$ and $y < 1$ separately. The region $y > 1$ may be regarded as a closed basin with an unknown condition on the boundary $y = 1$, so the solution in this region may be expected to have properties in common with the solution found by Stommel (1948) for a closed basin. As $\delta \to 0$, the latter solution tends to a solution of the parabolic equation

$$\delta\psi_{yy} + \psi_x = -X'(y), \tag{3.2}$$

except at the western boundary where a boundary layer of thickness of order δ develops and the solution tends to a solution of

$$\delta\psi_{xx} + \psi_x = 0. \tag{3.3}$$

The appropriate solution ψ_{MS} of (3.2) can be expressed as a power series in $\epsilon = \delta\ell$, with Sverdrup's (1947) solution as the leading term, namely

$$\psi_{MS} = (\ell - x)X'(y) + \delta(\ell - x)^2 X'''(y)/2! + \delta^2(\ell - x)^3 X^V(y)/3! + \ldots. \tag{3.4}$$

It is convenient to refer to this solution as the modified Sverdrup solution.

If ψ_{MS} does not happen to satisfy the appropriate conditions on $y = 1$ and $y = d$, a correction ϕ must be added to ψ_{MS}, so let

$$\psi = \psi_{MS} + \phi \quad \text{for} \quad y > 1, \tag{3.5}$$

or rather, let $\psi - \phi$ be a solution of the full equation (2.13) which tends to ψ_{MS} as $\delta \to 0$. Then ϕ satisfies the homogeneous equation

$$\delta(\phi_{xx} + \phi_{yy}) + \phi_x = 0, \tag{3.6}$$

vanishes on $x = 0,\ \ell$, and has given values on $y = 1, d$. Eckhaus & de Jager (1966, §4) have shown that, except at the western boundary, such solutions tend to solutions of the homogeneous parabolic equation

$$\delta\phi_{yy} + \phi_x = 0 \tag{3.7}$$

as $\delta \to 0$, and that errors are of order $(\delta/\ell)^{\frac{1}{2}}$. The solutions of (3.7) become small outside layers defined by

$$\left.\begin{aligned} (y-1)[\delta(\ell-x)]^{-\frac{1}{2}} &= O(1) \\ \text{and} \qquad (d-y)[\delta(\ell-x)]^{-\frac{1}{2}} &= O(1). \end{aligned}\right\} \tag{3.8}$$

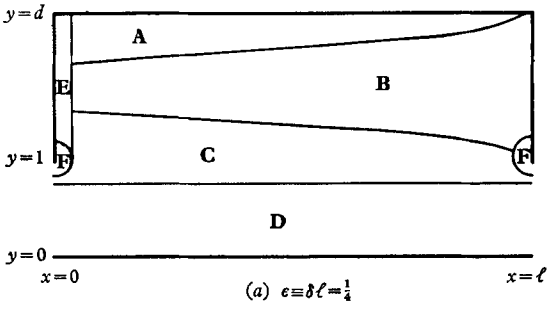

(*a*) $\epsilon \equiv \delta\ell = \frac{1}{4}$

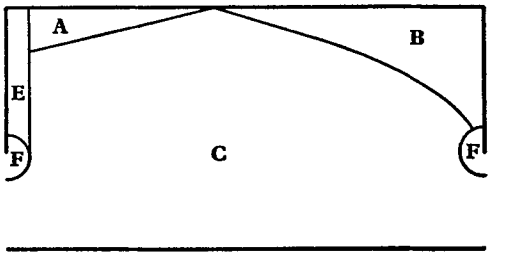

(*b*) $\epsilon \equiv \delta\ell = 1$

FIGURE 2. A schematic picture of the boundary layers that exist when the friction parameter δ is small. (*a*) is the case where the product $\delta\ell$ is also small, (*b*) the case where $\delta\ell$ is of order unity. The layers **E** and **F** are of thickness δ while **A** and **C** have average thickness of order $(\delta\ell)^{\frac{1}{2}}$. The Sverdrup (or in case (*b*) the modified Sverdrup) solution is valid in **B** while the zonal solution in valid in **D**. The western boundary current flows in **E**. The behaviour of the transport lines in **F** is shown in figure 8.

When ϵ is small, the layers are thin. Figure 2(*a*) shows the situation for small ϵ. In the region marked **B** the Sverdrup solution is a good approximation. **A** and the northern part of **C** are the boundary layers defined by (3.8) while **E** is the layer of thickness of order δ on the western boundary. If

$$\psi = \psi_{MS} \quad \text{on} \quad y = d, \tag{3.9}$$

the layer marked **A** is not present. It is useful on occasions to apply the condition (3.9) on $y = d$ instead of the condition $\psi = 0$ so that the solution is virtually independent of the value of d.

Consider now the region $y < 1$. This may be regarded as a zonal channel with an unknown condition on the line $y = 1$. It may be expected that the solution tends to the zonal solution

$$\psi_{\text{zonal}} = \psi_{\text{tot}} - \int_0^y X(y)dy/\delta \tag{3.10}$$

as $\epsilon \to 0$ except near the line $y = 1$. Near that line a correction of ϕ must be added, so let

$$\psi = \psi_{\text{zonal}} + \phi \quad \text{for} \quad y < 1. \tag{3.11}$$

ϕ must satisfy the homogeneous equation (3.6), be periodic in x with period ℓ and have given values on $y = 1$. If δ/ℓ is small, the solutions are close to solutions of the parabolic equation (3.7) and (Carslaw & Jaeger 1959, §2.6) are expressible as a sum of terms proportional to

$$\phi = \exp\left[i2\pi nx/\ell + (1-i)(n\pi/\delta\ell)^{\frac{1}{2}}(y-1)\right], \tag{3.12}$$

where n is an integer. These terms vanish outside a boundary layer of thickness of order $\epsilon^{\frac{1}{2}}$. This layer is shown as the southern part of the region marked **C** in figure 2(*a*), leaving a region **D** in which the zonal solution is a valid first approximation. Thus the composite picture for small ϵ is rather complicated with the solution being approximated either by the Sverdrup solution (region **B**) or the zonal solution (region **D**) except in the boundary layers **A**, **C**, **E** and **F**. If ϵ is not small, there is still a structure due to δ being small, as shown in figure 2(*b*). As $\delta \to 0$, the solution approaches a solution of the parabolic equation (3.2) everywhere except in the boundary layers **E** and **F**. It is still possible to distinguish a region **B** in which the modified Sverdrup solution is a first approximation, but this may only include part of any line $y =$ constant. Thus even if the boundary condition (3.9) is used on $y = d$, the solution will still depend on d in the region marked **A** in figure 2(*b*), the boundary of **A** being the reflexion of the first of the curves (3.8) in $y = d$. For the dependence on d to be weak it is necessary that $(d-1)\epsilon^{-\frac{1}{2}}$ be above a certain value.

Consider now how the total transport ψ_{tot} depends on δ and ℓ when δ is small. Solutions of the parabolic equation (3.2), which approximate solutions of the full equation over most of the domain of interest, have the property that ψ/ℓ depends only on x/ℓ, y and $\epsilon = \delta\ell$. Thus, to first order, ψ_{tot}/ℓ depends only on ϵ. Errors for small δ, are of two types. One error, of order $(\delta/\ell)^{\frac{1}{2}}$, is due to the term neglected in the governing equation, and another error is due to the boundary layers **E** and **F**. The latter errors may be expected to tend to zero in a similar manner to $\exp(-2/\delta)$.

The way ψ_{tot}/ℓ depends on ϵ for small ϵ will be found in §5 by matching solutions valid in the regions marked **B**, **C** and **D** in figure 2(*a*). It is assumed, however, that terms of the form (3.12) are small near $y = 0$, or rather, accounting for properties of symmetry about $y = 0$, at $y = -1$. The errors involved are proportional to

$$\exp\left[-2(n\pi/\epsilon)^{\frac{1}{2}}\right], \tag{3.13}$$

which is less than $\exp(-1)$ for all positive integers n if ϵ is less than 4π.

The next two sections are more or less independent of each other. The numeri-

cal results are presented first (§4) because they were obtained first and helped in the formulation of the ideas which led to the analytical solution discussed in §5.

4. Numerical solutions

A series of numerical solutions to the governing equation (2.13) were obtained by Dr J. W. Elder (see Elder 1968) using a general system for solving elliptic differential equations in two dimensions. The wind stress was assumed to have the form $X = X(y)$, $Y = 0$, with the following distributions for X as a function of y:

$$X = X_0 + \frac{6}{\pi} \sin\left(\frac{\pi}{4} + \frac{\pi y}{6}\right), \tag{4.1}$$

$$X = X_0 + \frac{5}{\pi} \sin\frac{\pi y}{5}, \tag{4.2}$$

and

$$X = X_0. \tag{4.3}$$

In each case X_0 is a constant. The first corresponds to having a maximum wind stress at 54·4° S and a separation between maximum and minimum stress of 26·4°. The second has a maximum at 50° S and a separation between the latitudes of maximum and minimum stress of 22°. The boundary condition (3.18) was applied at $y = d$.

The results are shown in table 1 and in figures 3 and 5. The results will be discussed first and the choice of parameters discussed later. Figures 3(*a*), (*b*) and (*c*) show how the solution depends on ϵ for a fixed wind stress distribution while comparison of 3(*b*) with 3(*d*) or 5(*a*) with 5(*b*) shows the dependence on wind stress pattern for a fixed ϵ. For comparison, a smoothed and simplified version of the transport lines as given by Kort (1962) is shown in figure 4. So that a quantitative comparison can be made, it is assumed that the quantity $T\ell/\beta$ by which the number ψ_{tot}/ℓ must be multiplied to give the transport through the passage in dimensional terms is equal to 3×10^8 m^3/s. This corresponds to half the difference between the maximum and minimum wind stress being 1·6 dyne cm^{-2} for the distribution (4.1) and 1·3 dyne cm^{-2} for (4.2).

Consider first figure 3. Figures 3(*a*), (*b*) and (*c*) correspond to the wind stress distribution (4.1) with $X_0 = 0$ while 3(*d*) corresponds to (4.2) also with $X_0 = 0$. The values of ϵ are shown. Comparison of figures 3(*a*), (*b*) and (*c*) shows that as ϵ increases, the current becomes both broader and weaker. The weakening of the current is due to the increased frictional stress while the broadening is due to the increase in thickness of the boundary layer marked **C** in figure 2. The east–west asymmetry is apparent in all cases, this being associated with the formation of a western boundary current. In the interior of the basin, the current is relatively broad and moves southwards as well as eastwards, narrowing as it approaches the passage. The convergence of the transport lines is particularly marked at the northern end of the passage indicating very strong currents there. These currents lead into a northward-flowing boundary current which is also intense and feeds the broader current in the interior.

The pattern deduced from observations by Kort has similar features, the main difference apparently being due to the presence of New Zealand and the shallow

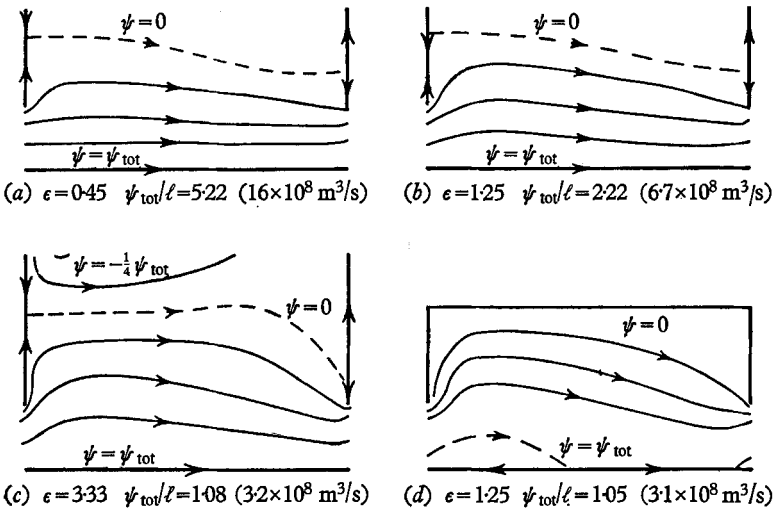

FIGURE 3. Some numerical solutions showing the dependence on the friction parameter ϵ [(*a*), (*b*), (*c*)] and on the wind stress distribution $X(y)$ [(*b*) and (*d*)]. X is given by (4.1) in cases (*a*), (*b*) and (*c*) and by (4.2) in case (*d*), X_0 being zero. The maximum wind stress is further north in the case (*d*). The contour interval for ψ is $\frac{1}{4}\psi_{tot}$. The figures in brackets represent the equivalent dimensional transport, Ψ_{tot}.

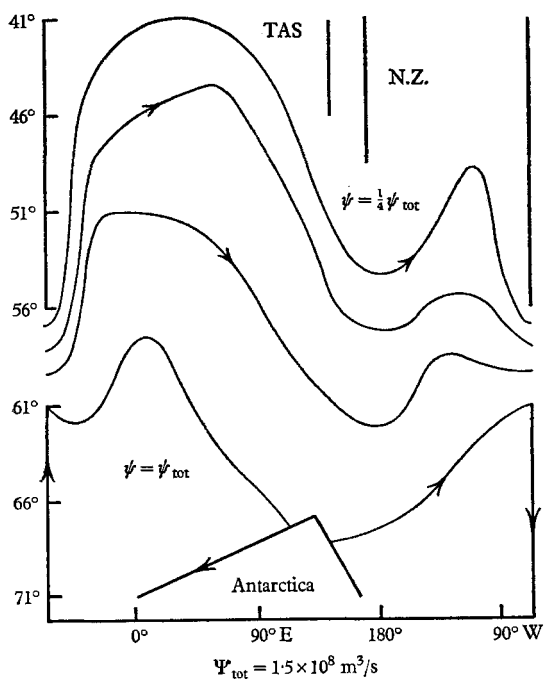

FIGURE 4. Transport lines after Kort (1962). The north–south scale has been exaggerated and the lines have been smoothed somewhat.

area to the south. The current is broader and weaker than those shown in figures 3(*a*), (*b*) and (*c*) suggesting a higher value of the friction parameter. The tendency for currents to be much stronger at the northern end of the passage has been noted by Gordon (1967).

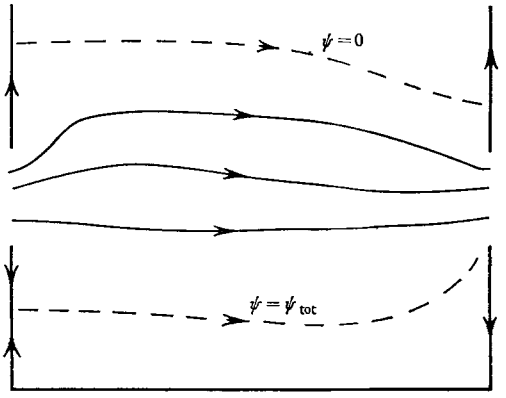

(*a*) $X_0 = 0$ $\psi_{tot}/\ell = 1{\cdot}91$ ($5{\cdot}7 \times 10^8$ m^3/s)

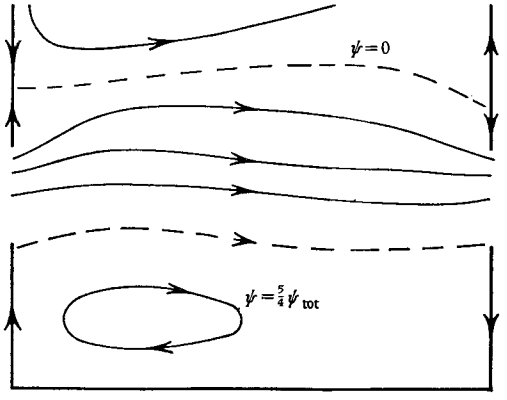

(*b*) $X_0 = -0{\cdot}9, \psi_{tot}/\ell = 0{\cdot}65$ (2×10^8 m^3/s)

FIGURE 5. Two numerical solutions for a different geometry, the wind stress being given by (4.1). The second shows the effect of adding a uniform westward stress. $\epsilon = 1{\cdot}8$ in both cases, and the figures in brackets represent the total dimensional transport, Ψ_{tot}.

Comparison of figure 3(*d*) with 3(*b*) shows the effect of moving the wind stress pattern to the north, or more precisely, replacing the pattern (4.1) with $X_0 = 0$ by (4·2) with $X_0 = 0$. The current is weakened because the stress in the latitudes of the passage is less. An interesting feature is the weak gyre in the south-west corner in which currents are partly moving against the wind.

The results for a different geometry are shown in figure 5. The boundary which corresponds to Antarctica was moved south to $y = 1 - d$. This geometry is perhaps more like that of the Southern Ocean with the boundary $x = \ell, y < 0$ playing a role similar to that of Graham Land. The current still tends to be north of the latitude of the centre of the passage because the wind stress is stronger to

the north. There is a weak westwards flow near the southern boundary due to the easterly winds there, and figure 5(*b*) shows how this westwards flow is intensified if the easterly wind is made stronger. (Note that easterly means *from* the east.)

Run	ϵ	Wind stress	Southern boundary	ψ_{tot}/ℓ'	δ	$d-1$	δN	X_0	Convergence error (%)	Theoretical ψ_{tot}/ℓ'
1	1·25	(4·2)	$y = 0$	2·00	0·25	1·5	2	0·725	±0·01	2·46
2	1·25	(4·2)	$y = 0$	1·60	0·20	1·5	1·6	0·38	±3·3	1·91
3	1·25	(4·1)	$y = 0$	2·25	0·25	1·5	2	0·026	±0·02	2·65
4	1·25	(4·3)	$y = 0$	0·50	0·25	1·5	2	0·381	±0·02	0·586
5	0·45	(4·1)	$y = 0$	6·25	0·15	1·5	1·8	0·33	±5·5	7·07
6	0·45	(4·1)	$y = 0$	0	0·15	1·5	1·8	−1·68	±2·2	0·12
7	3·33	(4·1)	$y = 0$	1·00	0·33	2·33	2	−0·122	±0·04	1·07
8	3·33	(4·1)	$y = 0$	0	0·33	2·33	2	−1·69	±0·5	−0·24
9	1·8	(4·1)	$y = 1-d$	2·67	0·30	1·5	1·8	0·545	±0·6	3·24
10	1·8	(4·1)	$y = 1-d$	0	0·30	1·5	1·8	−1·37	±0·7	−0·18
11	0·8	(4·3)	$y = 0$	1	0·40	1·0	2	0·602	<0·01	
12	0·8	(4·3)	$y = 0$	1	0·40	1·0	4	0·590	<0·01	
13	0·8	(4·3)	$y = 0$	1	0·40	1·0	6	0·586	0·03	

TABLE 1

Table 1 shows the parameters used for the actual computations. The first 10 runs are arranged in four groups for each of which ϵ was fixed. For each value of ϵ and type of wind distribution, (4.1) or (4.2), it was arranged that when the solution was known for one value of X_0, the solution for any other value of X_0 could be found by combining that solution with another in the same group.

Since ψ/ℓ depends mostly on $\epsilon = \delta\ell$, x/ℓ and y, the dependence on δ/ℓ being weak, values of ℓ more convenient for computation than the actual value could be used. This weak dependence on δ/ℓ, however, does not apply in the narrow region of the western boundary current so the transport lines shown in the figures may be distorted there. A test of the dependence of the solution on δ/ℓ was made in runs 1, 2 and 4. Comparison of the results of run 2 with a linear combination of the results of runs 1 and 4 shows that a change of 50 % in δ/ℓ makes a change in ψ_{tot}/ℓ of only 3 %. The distortion of the western boundary current is mainly a change of width only. In all the computations, except the test runs 11–13, δ/ℓ was kept below 1/20, and δ below $\frac{1}{3}$. In order for dependence on d to be weak $(1-d)\epsilon^{-\frac{1}{2}}$ was kept above unity.

Runs 11–13 were designed to test dependence on the numerical parameter N which is the number of grid intervals across the gap. The parameter δN shown in the table is the width of the western boundary current in grid intervals. This had to be above 1·5 for the numerical scheme to converge. Runs 11–13 indicate an error in X_0 of about 3 % when δN is 2. Also shown is the 'convergence error'

in the value of ψ at the centre of the grid. This value was printed after each iteration involved in the numerical scheme and usually showed a damped oscillation. The convergence error indicates the amplitude of oscillation at the last iteration. Another indication of the numerical error due to the small value of δN used was provided by the integral (2.14) which was used to calculate the value of X_0. The calculation was made for different values of y between 0 and 1. The value at one grid point from $y = 1$ was always higher than values near $y = 0{\cdot}5$ by up to 0·014 although values for y near 0·5 varied by less than 0·002. The improvement with increase of δN showed up in runs 11 to 13 in which the maximum differences of this type were respectively 0·006, 0·004 and 0·001.

5. An analytic solution for small friction

The problem of finding solutions analytically is not as straightforward as it might be because of the unusual geometry involved. The aim of this section is to find, for small values of ϵ, the function ϕ defined by (3.5) and (3.11). This function satisfies to first order as $\delta \to 0$, the parabolic equation (3.7) and vanishes outside the region marked **C** in figure 2(*a*). As indicated in §3, terms of order (3.13) will be neglected so that the fractional error may be expected to be less than e^{-1} if ϵ is less than 12. It is helpful to use boundary-layer co-ordinates defined by

$$\left.\begin{aligned} \xi &= (\ell - x)/\ell, \\ \eta &= (y-1)/\epsilon^{\frac{1}{2}}. \end{aligned}\right\} \tag{5.1}$$

Then (3.7) takes the form

$$\phi_{\eta\eta} - \phi_\xi = 0, \tag{5.2}$$

which involves no parameters explicitly. The parameter ϵ only arises when the matching condition at $y = 1$ is brought in. This condition is that ψ and ψ_y are continuous at $y = 1$, the relation between ϕ and ψ being given by (3·5) and (3.11). The series form (3.4) of ψ_{MS} and the integral form (3.11) for ψ_{zonal} may be used to express ψ_{MS} and ψ_{zonal} as power series in ϵ valid for ξ, η of order unity. Thus the relations (3.11) and (3.5) may be written

$$\left.\begin{aligned} \frac{\psi}{\ell} &= \frac{\psi_{\text{tot}}}{\ell} - \frac{1}{\epsilon}\int_0^1 X(y)\,dy - \epsilon^{-\frac{1}{2}}X(1)\eta - X'(1)\eta^2/2\,! - \ldots + \frac{\phi}{\ell} \quad \text{for} \quad \eta < 0, \\ \frac{\psi}{\ell} &= X'(1)\xi + \epsilon^{\frac{1}{2}}X''(1)\xi\eta/2\,! + \epsilon X'''(1)(3\xi^2 + \xi\eta^2)/3\,! + \ldots + \frac{\phi}{\ell} \quad \text{for} \quad \eta > 0. \end{aligned}\right\} \tag{5.3}$$

Note that for each non-negative integer m, $\epsilon^{\frac{1}{2}(m-1)}$ is multiplied by the m^{th} derivative $X^{(m)}$ of X at $y = 1$. This fact enables variables to be written in the following simple series forms

$$\psi_{\text{tot}}/\ell = \int_0^1 X(y)\,dy/\epsilon + \sum_{m=0}^{\infty} \sigma_m \epsilon^{\frac{1}{2}(m-1)} X^{(m)}, \tag{5.4}$$

$$\left.\begin{aligned} \phi/\ell &= \sum_{m=0}^{\infty} \phi_m \epsilon^{\frac{1}{2}(m-1)} X^{(m)}, \\ \psi/\ell &= \sum_{m=0}^{\infty} \psi_m \epsilon^{\frac{1}{2}(m-1)} X^{(m)}. \end{aligned}\right\} \tag{5.5}$$

Each ϕ_m is a function of ξ, η only and each σ_m is a constant. ϕ_m and σ_m do *not* depend on ϵ or the wind stress. As soon as ϕ_m and σ_m have been determined, the total transport can be calculated for any small ϵ and any wind stress distribution $X(y)$ using (5.4) and the transport function can be calculated using (5.3) and (5.5).

The equations and boundary conditions to be satisfied are as follows. Each ϕ_m satisfies equation (5.2), tends to zero as $|\eta| \to \infty$, vanishes on $\xi = 0$ for $\eta > 0$ and is periodic in ξ with unit period for $\eta < 0$. In addition there is the requirement of continuity of ψ and ψ_η on $\eta = 0$ and the condition (2.14) for continuity of the pressure field. The condition at $\eta = 0$ follows from substitution of (5.4) and (5.5) in (5.3). Using the affix + to denote a value at $\eta = 0+$ and the affix − for a value at $\eta = 0-$, these conditions may be written

$$\psi_m = \phi_m^- + \sigma_m = \phi_m^+ + \delta_{m-1,e}\xi^{\frac{1}{2}(m+1)}/\Gamma[\tfrac{1}{2}(m+3)], \tag{5.6}$$

$$\psi_{m\eta} = \phi_{m\eta}^- - \delta_{m0} = \phi_{m\eta}^+ + \delta_{me}\xi^{\frac{1}{2}m}/\Gamma[\tfrac{1}{2}(m+2)] - \delta_{m0}, \tag{5.7}$$

where

$$\delta_{me} = \begin{cases} 1 & \text{if } m \text{ is even,} \\ 0 & \text{if } m \text{ is odd.} \end{cases}$$

The pressure continuity condition (2.14) applied at $\eta = 0-$ leads to the conditions

$$\int_0^1 \phi_{m\eta}^- d\xi = 0. \tag{5.8}$$

The method of solution consists of finding relations between ϕ^+ and $\phi_{m\eta}^+$ and between ϕ_m^- and $\phi_{m\eta}^-$ which, used in conjunction with (5.6), (5.7) and (5.8) yield the solution. These relations may be obtained from well-known solutions of the heat equation (5.2), given, for instance, in Carslaw & Jaeger (1959, chapter 2). In particular, use will be made of the fundamental solution

$$\phi = \begin{cases} (\xi - t)^{-\frac{1}{2}} \exp[-\eta^2/4(\xi - t)] & (\xi > t), \\ 0 & (\xi < t). \end{cases} \tag{5.9}$$

For thermal problems this solution is well known as that corresponding to an instantaneous plane source of heat. In the ocean current problem it represents the (approximate) solution due to a concentrated point, or δ-function distribution, of wind stress curl applied at $\xi = t$, $\eta = 0$. Such a distribution has been called a wind stress 'tweak' by Longuet-Higgins (1965). The function ϕ in the region $\eta > 0$ is proportional to the transport function distribution induced by a set of wind stress tweaks of strength $\phi_\eta^+(t)$ distributed along the line $\eta = 0$. Thus (Carslaw & Jaeger 1959, chapter 2)

$$\phi = -\pi^{-\frac{1}{2}} \int_0^\xi \phi_\eta^+(t)(\xi - t)^{-\frac{1}{2}} \exp[-\eta^2/4(\xi - t)]\, dt \tag{5.10}$$

for $\eta > 0$, and similarly

$$\phi = \pi^{-\frac{1}{2}} \int_{-\infty}^\xi f(t)(\xi - t)^{-\frac{1}{2}} \exp[-\eta^2/4(\xi - t)]\, dt \tag{5.11}$$

for $\eta < 0$, where

$$f(t) = \begin{cases} \phi_\eta^-(t) & (t > 0), \\ \phi_\eta^-(n + t) & (-n < t < -n + 1; n = 1, 2, \ldots). \end{cases}$$

The latter form (5.11) arises because of the periodicity condition. Applied at $\eta = 0$ in particular these give the desired relations:

$$\phi^+ = -\pi^{-\frac{1}{2}} \int_0^\xi \phi_\eta^+(t)(\xi - t)^{-\frac{1}{2}} dt, \tag{5.12}$$

$$\phi^- = \pi^{-\frac{1}{2}} \int_{-\infty}^\xi f(t)(\xi - t)^{-\frac{1}{2}} dt. \tag{5.13}$$

The second integral (5.13) converges because of (5.8). It is in a form which is awkward to exploit as it stands because it involves the function $f(t)$ so (5.13) will be replaced by an equivalent set of properties of the integral. The first property is that the mean value of ϕ^- is zero,

$$\int_0^\xi \phi^-(\xi) d\xi = 0, \tag{5.14}$$

which is a consequence of (5.8) and the periodicity of ϕ^-, and can be proven using (5.13). The other property that will be used is

$$\phi^-(1+\xi) - \phi^-(\xi) = \pi^{-\frac{1}{2}} \int_0^\xi [\phi_\eta^-(1+t) - \phi_\eta^-(t)](\xi - t)^{-\frac{1}{2}} dt, \tag{5.15}$$

which follows directly from (5.11) and (5.13). Strictly speaking ϕ^- and ϕ_η^- are not defined at $1+\xi$ so are to be regarded as analytic continuations of ϕ^- and ϕ_η^- as defined on $0 < \xi < 1$. The properties (5.14) and (5.15) will be used in place of (5.13) and regarded as equivalent.

Substituting the expressions for ϕ^- given by (5.6) in (5.14) and (5.15) and use of (5.12) leads to the equations

$$\sigma_m = -\pi^{-\frac{1}{2}} \int_0^1 \int_0^\xi \phi_\eta^+(t)(\xi - t)^{-\frac{1}{2}} dt\, d\xi + \delta_{m-1,e}/\Gamma[\tfrac{1}{2}(m+1)] \tag{5.16}$$

and

$$\pi^{-\frac{1}{2}} \int_0^\xi [\phi_\eta^-(1+t) - \phi_\eta^-(t)](\xi - t)^{-\frac{1}{2}} dt = -\pi^{-\frac{1}{2}} \int_\xi^{1+\xi} \phi_{m\eta}^+(t)(\xi - t)^{-\frac{1}{2}} dt + \delta_{m-1,e} \frac{(1+\xi)^{\frac{1}{2}(m+1)} - \xi^{\frac{1}{2}m}}{\Gamma[\frac{1}{2}(m+3)]}. \tag{5.17}$$

In order to solve these, it is convenient to express $\phi_{m\eta}^-$ as a power series in $\xi^{\frac{1}{2}}$, namely

$$\phi_{m\eta}^- = \sum_{r=0}^\infty \phi_{mr} \xi^{\frac{1}{2}(r-1)}/\Gamma[\tfrac{1}{2}(r+1)]. \tag{5.18}$$

A similar series for $\phi_{m\eta}^+$ follows from (5.7). Substituting in (5.16) gives

$$\sigma_m = -\sum_{r=0}^\infty \phi_{mr}/\Gamma[\tfrac{1}{2}(r+4)] + 1/\Gamma[\tfrac{1}{2}(m+5)], \tag{5.19}$$

while substitution in (5.17) gives, equating coefficients of $\xi^{\frac{1}{2}s}$

$$\sum_{r=0}^\infty \phi_{mr} \frac{(1 - 2\delta_{sr})}{\Gamma[\frac{1}{2}(r+2-s)]} = \frac{\delta_{se} - \delta_{s,m+1}}{\Gamma[\frac{1}{2}(m+3-s)]} \tag{5.20}$$

for $s = 0, 1, 2, \ldots$. In addition, condition (5.8) gives

$$\sum_{r=0}^\infty \phi_{mr}/\Gamma[\tfrac{1}{2}(r+3)] = 0, \tag{5.21}$$

which is the same as (5.19) for $s = -1$.

The procedure for solving the matrix equation (5.20) with $r, s+1$ ranging from 0 to ∞ was simple truncation, allowing the indices $r, s+1$ to range only from 0 to M. The truncated matrix equation was solved on the TITAN computer at Cambridge. Convergence was quite good for small values of r but not so good for the larger values. For instance, the results for ϕ_{m0} $(m < 10)$ for $M = 16$ and $M = 23$ agreed to 4 figures while values of $\phi_{0r}(r > 6)$ sometimes differed by more than 10%. Some values, which agreed to the accuracy shown for $M = 16$ and $M = 23$, are:

$$\begin{aligned}
\phi_{0r} &= -0{\cdot}5000,\ 0{\cdot}6315,\ -0{\cdot}1357,\ 0{\cdot}062,\ 0{\cdot}066,\\
\phi_{1r} &= -0{\cdot}4120,\ 0{\cdot}1964,\ 0{\cdot}2567,\ 0{\cdot}187,\ -0{\cdot}007,\\
\phi_{2r} &= -0{\cdot}2947,\ 0{\cdot}1948,\ -0{\cdot}2764,\ 0{\cdot}780,\ -0{\cdot}148,\\
\phi_{3r} &= -0{\cdot}1887,\ 0{\cdot}1556,\ -0{\cdot}2460,\ 0{\cdot}300,\ 0{\cdot}245,\\
\phi_{4r} &= -0{\cdot}1103,\ 0{\cdot}1074,\ -0{\cdot}1856,\ 0{\cdot}260,\ -0{\cdot}285.
\end{aligned}$$

The values of ϕ_{mr} were then used to evaluate σ_m using (5.19) with summation from 0 to M only. Convergence was good with agreement between values obtained for $M = 16$ and 23 to 4 significant figures for all values of m up to 16. The values up to $m = 11$ are:

$$\begin{aligned}
\sigma_m = {} & 0{\cdot}8239,\ 0{\cdot}5894,\ 0{\cdot}3774,\ 0{\cdot}2206,\ 0{\cdot}1193,\ 0{\cdot}0603,\\
& 0{\cdot}0288,\ 0{\cdot}0130,\ 0{\cdot}0056,\ 0{\cdot}0023,\ 0{\cdot}0009,\ 0{\cdot}0003.
\end{aligned}$$

These values can be used to calculate ψ_{tot}/ℓ as a function of ϵ and of the wind stress distribution using (5.4) The result can be extended by symmetry to the case where the southern boundary is not at $y = 0$ but sufficiently further south, as in figure 5. In this case ψ_{tot} is given by

$$\psi_{\text{tot}}/\ell = \int_0^1 X(y)\,dy/\epsilon + \sum_{m=0}^{\infty} \sigma_m \epsilon^{\frac{1}{2}(m-1)}(X^{(m)} + (-1)^m X_0^{(m)}), \tag{5.22}$$

where $X_0^{(m)}$ signifies the m^{th} derivative of $X(y)$ evaluated at $y = 0$ instead of at $y = 1$. In dimensional terms, the formula is

$$r\Psi_{\text{tot}} = \int_0^B X(y)\,dy + \sum_{m=0}^{\infty} \sigma_m (rL/\beta)^{\frac{1}{2}(m+1)}[X^{(m)}(B) + (-1)^m X^{(m)}(0)].$$

Figure 6 shows the values of ψ_{tot}/ℓ computed from both formulae (5.4) and (5.22) for the sinusoidal wind stress distribution

$$X = \frac{6}{\pi}\sin\left(\frac{p\pi}{36} + \frac{\pi y}{6}\right). \tag{5.23}$$

The wind stress has a maximum at $y = 3 - p/6$ and on figure 6 the corresponding latitude of maximum wind stress is shown assuming Drake Passage extends from 56·6° S to 61·0° S. The results shown here will be used as a basis for discussion in the next section.

The above results can also be used to find the pattern of the transport lines. To find ϕ for $\eta > 0$, (5.10) can be used. The necessary expression for ϕ_η^+ follows from (5.7) and (5.18). The result, written in terms of ψ is

$$\psi/\ell = \sum_{r=0}^{\infty} a_r (4\xi)^{\frac{1}{2}r} i^r \operatorname{erfc}(\eta/2\xi^{\frac{1}{2}}) + \psi_{ms}/\ell, \tag{5.24}$$

where the results of Carslaw & Jaeger (1959, §2.9) have been used and the error

function integrals are defined in appendix II of the same book. The coefficients a_r are defined by

$$a_r = -\sum_{m=0}^{\infty} \phi_{mr} \epsilon^{\frac{1}{2}(m-1)} X^{(m)} + \delta_{r-1,e} \epsilon^{\frac{1}{2}(r-2)} X^{(r)}. \tag{5.25}$$

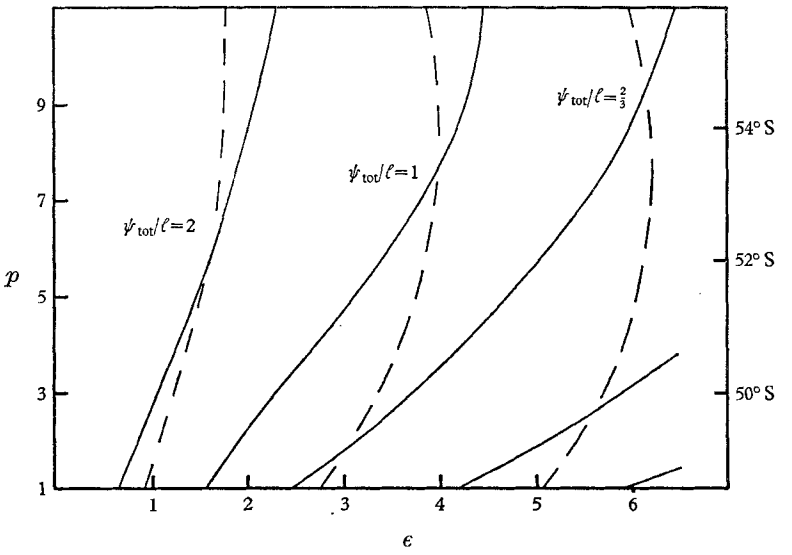

FIGURE 6. ψ_{tot}/ℓ as a function of the friction parameter ϵ and the wind stress distribution given by (5.23). The latitude of maximum stress for each distribution is indicated at the right. The contour interval for ℓ/ψ_{tot} is $\frac{1}{2}$. The broken lines correspond to the geometry of figure 3, the contours being calculated by (5.4). The solid contours correspond to the geometry of figure 5 and are calculated by (5.22).

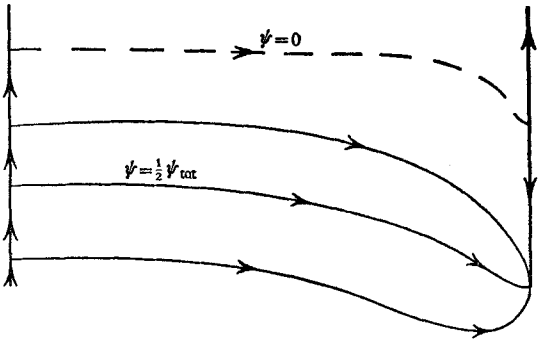

FIGURE 7. Transport lines given by the analytical solution (5.24) for $\epsilon = 6$ and $p = 3$. The value of ψ_{tot}/ℓ given by (5.4) is 0·63 and the value of a_0 is 0·27.

Although the solution (5.24) has been derived for $\eta > 0$ it is valid also for $\eta < 0$ by analytical continuation. The pattern given by the above expression is shown in figure 7 for the wind stress pattern (5.23) with $\epsilon = 6$ and $p = 3$. This case was selected as giving a realistic total transport with a wind stress pattern close to the actual one, and the transport lines may be compared with the observed ones in figure 4.

The above solution is not valid in the thin boundary regions **E** and **F**, so different expressions will be needed there. The appropriate solution in **E** is well known as a western boundary current, and satisfies (3.3). The solution in **F** is not so easy to obtain as only the forcing term on the right-hand side of the full equation (2.13) can be ignored near there, so that the approximate equation has

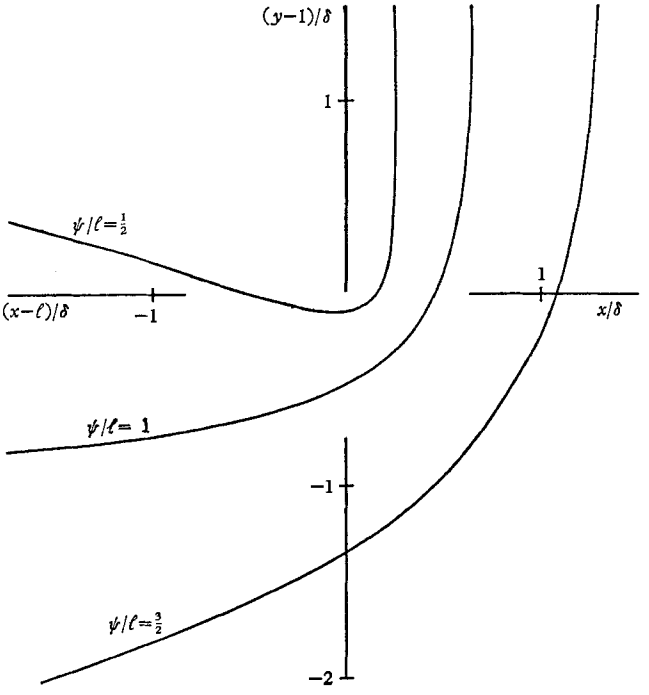

FIGURE 8. Transport lines, as given by (5.28), near the tip of the peninsula which corresponds in the model to Cape Horn. There is a transport of $2a_0$ which goes into a 'western boundary current' seen here to the right of the diagram. There is no exaggeration of the north–south scale.

the form (3.6). It is necessary to find a solution of this equation which satisfies the boundary condition on $x = 0, \ell$; $y > 1$ and has the same asymptotic form away from the singularity as (5.24) does near the singularity ($\xi, \eta \to 0$), that is

$$\psi/\ell \sim a_0 \operatorname{erfc}(\eta/2\xi^{\frac{1}{2}}). \tag{5.26}$$

The appropriate solution of (3.6) can be obtained in terms of parabolic co-ordinates u, v defined as follows

$$\left.\begin{aligned} u^2 - v^2 &= \begin{cases} (\ell - x)/\delta = \ell\xi/\delta = \epsilon\xi/\delta^2 & (x > \frac{1}{2}\ell), \\ -x/\delta = \epsilon(\xi - 1)/\delta^2 & (x < \frac{1}{2}\ell), \end{cases} \\ 2uv &= (y-1)/\delta = \epsilon^{\frac{1}{2}}\eta/\delta. \end{aligned}\right\} \tag{5.27}$$

The co-ordinates are defined in a way which puts the point $x = 0, \ell; y = 1$ at the centre. It is also necessary to give a sign convention as the above definition is not unique. A suitable convention is $u, v > 0$ for $\xi, \eta > 0$, $u > 0$, $v < 0$ for $\eta < 0$ and $u, v < 0$ for $\xi < 1$, $\eta > 0$. The co-ordinates are discontinuous on the line

which corresponds to the South American peninsula. $u = v > 0$ corresponds to the east coast and $u = v < 0$ to the west coast of the peninsula. The equation (3.6) when written in terms of the parabolic co-ordinates is separable and solutions for the separated equations can be written in terms of error function integrals, $i^n \operatorname{erfc}(z)$ and Hermite polynomials, $H_n(z)$ (Erdélyi 1953, volume 2). The solution which satisfies the boundary conditions on $u = v$ and asymptotes to (5.26) as $u, v \to \infty$ is

$$\psi/\ell = a_0[\operatorname{erfc}(v) - e^{u^2-v^2}\operatorname{erfc}(u)]. \tag{5.28}$$

This equation gives the pattern of transport lines near the point $\xi = 0, 1; \eta = 0$, as shown in figure 8. The currents are very strong in this neighbourhood and are in fact infinite at the tip of the peninsula. A transport of $a_0\ell$ passes within a distance of $\frac{1}{2}\delta$ of the tip of the peninsula. Note also that there is no exaggeration of the north–south scale in this diagram so the transport lines to the west of the peninsula do not appear to converge as rapidly as in previous figures.

(5.28) also allows an estimate to be made of the error involved in using the approximate equation (5.2). The difference between the expressions (5.26) and (5.28) for ψ/ℓ at $\xi = 1, \eta = 0$ is approximately $a_0(\delta/\pi\ell)^{\frac{1}{2}}$. This should be compared with the value of $2a_0$ for ψ/ℓ given by (5.24) at the same point so the percentage error there is $(\delta/4\pi\ell)^{\frac{1}{2}}$, and so less than 7 % if δ/ℓ is less than $\frac{1}{20}$ as in the computations, and less than 2 % if $\ell = 42$ and $\epsilon < 8$ as may be expected to hold in practice. Errors in ψ_{tot} would be expected to be no greater.

6. Evaluation of the results

The results suggest a value of ϵ between 4 and 6 which indicates a fairly strong coupling between the currents at different latitudes. An indication of this is that the first term in the expression (5.4) for the total transport, that is the zonal transport term, represents only 25 to 40 % of the total transport. The greater part of the transport is due to frictional coupling with the currents to the north which are driven by strong westerlies. Comparison of the results for the figure 1 geometry with those for the figure 5 geometry indicate that frictional coupling with currents to the south can *decrease* the total transport due to the easterly winds there, but this effect is probably not strong in practice because the easterlies are relatively weak. The strength of the coupling also means that a large proportion of the water going through the passage is directed into the western boundary current. The proportion is given by $2a_0\ell/\psi_{\text{tot}}$ and for the case $p = 3$, $\epsilon = 6$ shown in figure 6 is about $\frac{6}{7}$, that is, all but $\frac{1}{7}$ of the water passing through the passage goes into the western boundary current and moves north of the latitude of Cape Horn. This feature is also apparent in the observations (figure 4). A concentration of the currents at the north end of Drake Passage is also indicated. The current distribution inferred for observations by Gordon (1967) shows the same feature. The conclusion is not altered when the figure 5 geometry is used because the easterlies to the south are weak compared with the westerlies to the north. Also the water to the south is often shielded from the wind by ice.

The largish value of ϵ also implies the western boundary current goes well to the north of the passage resulting in a strong east–west asymmetry in the pattern of transport lines. Comparison of the calculated results in figures 3, 5

and 6 with figure 4, however, suggests that in actual practice the asymmetry is even stronger. The other significant difference between observation and calculation is the appearance of kinks in the transport lines to the south of New Zealand. This is clearly associated with the presence of New Zealand since addition of another meridional barrier in the model to correspond to New Zealand would lead to the same effect. Possible explanations of the greater asymmetry are the effects of bottom topography, the non-zonality of the actual wind stress, and a poor representation of the friction processes. These three effects will now be considered in turn.

Effect of bottom topography

The effects of large scale bottom topography on the circumpolar current have been discussed by Kamenkovich (1962), who calculated the equivalent of the zonal transport term in the series (5.4) for ψ_{tot}/ℓ. The magnitude of this term is not strongly affected by the bottom topography but the course of the current can be shifted since there is a tendency to follow lines of constant f/h where h is the depth. These lines are parallels of latitude when the depth is constant. Kamenkovich shows in his figure 8 the contours of f/h when the larger scale depth variations are taken into account. These lines tend to be further north in the Atlantic segment than in the Pacific segment which means the currents would tend to go further north in the Atlantic as observed.

It should be noted, incidentally, that Kamenkovich used only the equivalent of the zonal transport term in the series (5.4). This gives a value of ψ_{tot} of the observed order for a value of ϵ between $\frac{1}{4}$ and $\frac{2}{5}$ of the value required when the full series is used. The corresponding value of eddy viscosity is lower by a factor of 6 to 16, which explains why Kamenkovich required an eddy viscosity of only $1{\cdot}4 \times 10^2$ cm^2/s to obtain a reasonable result.

Non-zonality of wind stress

The wind stress pattern appears to have a marked east–west asymmetry rather similar to that exhibited by the currents. This asymmetry is probably due to the effect of the Andes on the winds which resemble the effect of the South American peninsula on the currents. Wyrtki (1960) gives a map of the distribution of maximum westerly winds which shows the asymmetry quite clearly. The non-zonality of the wind stress pattern may be expected to increase the east–west asymmetry of the current pattern.

It is not difficult to incorporate the effects of non-zonality of the wind stress in the analytical solution. One can illustrate with the solution for one Fourier component of X of the form

$$X = \sin\left(\frac{2\pi n x}{\ell} + ky + \alpha\right),$$

where n is an integer. A wind stress distribution of this type was considered by Wyrtki (1960), who did not, however, take into account the effect of meridional barriers. The solution for the case where there are meridional barriers, but no east–west boundaries, is simply

$$\psi = \psi_P(x, y) - \psi_P(0, y) + \psi_1(x, y),$$

where ψ_P is the particular periodic solution of (2.13)

$$\psi_P(x,y) = \frac{mk\sin(mx+ky+\alpha) - \delta(m^2+k^2)\cos(mx+ky+\alpha)}{m^2+\delta^2(m^2+k^2)^2},$$
$$m = 2\pi n/\ell,$$

and ψ_1 is the solution of (2.13) for the zonal wind stress distribution

$$X_1 = -\delta\psi_{Py}(0,y).$$

If $\delta(m^2+k^2) \ll m$, as fits the case $n = 1$, $k = \frac{1}{6}\pi$, $\epsilon = 6$, then ψ_P is approximately the solution of Sverdrup's equation. The amplitude of ψ_P is k/m, which is small compared with the amplitude $1/\delta k$ for the corresponding zonal stress distribution $m = 0$. The ratio $\delta k^2/m$ is about $\frac{1}{4}$ for the case $n = 1$, $k = \frac{1}{6}\pi$, $\epsilon = 6$, and is smaller for larger values of n. Thus the contribution to ψ of the non-zonal part of the wind stress is small compared with the contribution from a zonal wind stress of the same amplitude and north–south wave-number.

The form of frictional resistance

The indicated value of ϵ of 4 to 6 corresponds to a width W of the western boundary current of 50–70 km. This may be compared with the value of 100 km which Stommel (1948) found gave a good fit to data for the North Atlantic. The coefficient of eddy viscosity given by (2.4) is between 10^3 and 2×10^3 cm^2/s and the corresponding thickness for an Ekman layer is 45–60 m. To obtain an idea of the importance the type of friction has on the calculations one can easily work out the form of solution for a lateral friction model and make comparisons. If the coefficient of eddy viscosity in the lateral-friction model is A, the equation analogous to (2.6) is

$$-A\nabla^4\Psi + \beta\Psi_x = Y_x - X_y.$$

The boundary conditions are the same as those in the bottom friction model except for the additional condition that normal derivations of Ψ must vanish on solid boundaries and the condition for continuity of pressure analogous to (2.7) is

$$A\int_0^L \Psi_{yyy}\,dx - \int_0^L X\,dx = 0 \quad \text{for} \quad 0 < y < B.$$

The structure of the solution is very similar to that shown in figure 2, the boundaries being defined in an analogous way. The e-folding distance W for the boundary layer corresponding to **E** in figure 2 is given by

$$W = 2\left(\frac{A}{\beta}\right)^{\frac{1}{3}}, \tag{6.1}$$

and there is a similar region adjacent to the eastern boundary. The associated non-dimensional parameter is

$$a = \frac{A}{\beta B^3} = \left(\frac{W}{2B}\right)^3.$$

Non-dimensional quantities may be defined by (2.12) as before, and the analogue of (5.4) is an expansion for ψ_{tot}/ℓ in integer powers of $(a\ell)^{\frac{1}{4}}$, the leading term corresponding to the zonal transport of order $(a\ell)^{-1}$. Both (5.4) and its analogue

may be regarded as power series in the average non-dimensional thickness, t, of the boundary-layer **C** which, on the basis of e-folding distances, is about $t = 1{\cdot}5(\delta\ell)^{\frac{1}{2}}$ in the bottom-friction model and about $t = 4(a\ell)^{\frac{1}{4}}$ in the lateral-friction model. The leading term, however, in the expansion for ψ_{tot}/ℓ is proportional to t^{-2} for the bottom-friction model and proportional to t^{-4} for the lateral-friction model. This difference does not seem to be very significant for the case in hand, however, since t is of order unity. If, for the wind stress distribution (5.23) with $p = 3$ to 5, the leading term in the expansion of ψ_{tot}/ℓ were dominant and $\psi_{\text{tot}}/\ell \sim \frac{2}{3}$, then $a\ell$ would be between 0·12 and 0·17 and t about 2·4. This indicates that frictional coupling is important and the remaining terms in the expansion of ψ_{tot}/ℓ are of the same order as the first. Assuming these terms add to ψ_{tot} as they do in the bottom-friction model, a larger value of a must be taken to make ψ_{tot}/ℓ about $\frac{2}{3}$. In dimensional terms, this means the eddy viscosity coefficient A must be greater than 3×10^7 cm^2/s. If, as in the bottom-friction model, the transport is about 3 times the zonal transport, then the appropriate value for A is about 10^8 cm^2/s. The factor 3 is only a guess but probably is the right order, since the non-dimensional friction layer width, t, is about the same as in the bottom-friction model. This also implies that the east–west asymmetry is about the same in the two models. The width W of a western boundary current for $A = 10^8$ cm^2/s is by (6.1), about 200 km. This is wider than in the bottom-friction model, so currents in regions **E** and **F** of figure 2 would be less intense than in the bottom-friction model.

Despite the difference between the two models, the conclusions reached are much the same. Both indicate a strong frictional coupling, this being indicated by the region **C** being about 3 times the width of the gap. The circumpolar current is thus several times wider than the gap and the transport a few times the zonal transport corresponding to the gap width. There is a significant difference between the two models, however, if time variations are considered. The time scale in the bottom-friction model is r^{-1} which is around 10^6 sec or 10 days, while for the lateral-friction model the time scale is L^2/A where L is an appropriate length scale. The thickness of the frictional coupling layer is over 1000 km and the corresponding time scale over 10^8 days or 3 years. In short, the lateral-friction model responds much more slowly to changes with time and would not reflect seasonal changes to the extent that a bottom-friction model would.

One would like to be able to draw firm conclusions as to the nature of the principal friction processes operating in the Southern Ocean from the above estimates of eddy viscosity, but both figures fall within the range of values found from direct observations (Defant 1961, volume I, chapter III, §2) so neither mechanism can be rejected from that viewpoint.

A more general comparison of the two processes can be made by considering the eastward components of forces acting on the volume of ocean bounded by 56·6° S, 61·0° S, the ocean surface and the ocean floor. This comparison does not rely on the concept of eddy viscosity or the use of a linear friction law. The question is: what is the most important force balancing the wind force of about 10^{17} dyne acting on the surface of the strip of ocean? If it is a frictional force on the bottom, the bottom stress must on average be of the same order, 1 dyne/cm^2,

as the surface stress, as indicated by (2.2). If the drag law relating the bottom stress to the bottom velocity is roughly given by (Defant 1961, volume 2, p. 514)

$$X_{\text{bottom}} = 0{\cdot}002\rho(v_{\text{bottom}})^2,$$

bottom velocities of around 20 cm/s would be required. Such large values would appear to be inconsistent with indirect evidence based on a comparison between the relative velocity field deduced from hydrographic observations and either direct measurements of surface drift velocities or the estimate by Gordon (1967) of the transport through Drake Passage. The alternative one has in mind when invoking a *lateral* friction process is that the wind force is balanced by a northward momentum flux out of the volume of ocean concerned. Since the area across which the flux takes place is about 10^{15} cm^2, a mean value of the flux $\rho\overline{uv}$ per unit area would need to be about 100 dyne/cm^2. Assuming that the principal part of $\overline{uv}$ is due to the fluctuations of u and v about their mean values, the magnitude of the fluctuations would need to be at least 10 cm/s, that is, of the same order as the mean velocity. Another force which acts on the volume is the Coriolis force due to the northward movement of water discharged from the Antarctic continent, but if the figure for the rate of discharge estimated by Barcilon (1966) is of the right order, this force is less than 10^{15} dyne and so may be neglected. Although by no means conclusive, the above evidence suggests that bottom friction is not of primary importance between the latitudes concerned, but that the flux of momentum across these latitudes is important.

In addition to the momentum flux due to fluctuations there is a flux due to the mean flow. This effect is not expected to be large and is ignored in the linearised equations. However, a scale analysis based on the solutions for the linear model does show that the non-linear 'inertial' terms neglected in the analysis are quite important in the regions marked **E** and **F** in figure 2, that is in the regions where the currents are strongest. This probably means that details in this region will be wrong, but not the overall picture. It also means that details of coastline shape and bottom topography to the south and east of southern South America have important effects on the currents there. These effects would make an interesting study, but are outside the scope of this paper.

Part of this work was carried out at the Institute of Geophysics and Planetary Physics at the University of California at San Diego, and supported there by the National Science Foundation under contract NSF-GP-2414.

REFERENCES

Barcilon, V. 1966 *J. mar. Res.* **24**, 269.
Barcilon, V. 1967 *J. mar. Res.* **25**, 1.
Carslaw, H. S. & Jaeger, J. C. 1959 *Conduction of Heat in Solids*, (2nd Edition). Oxford.
Crease, J. 1964 *Proc. R. Soc.* A, **281**, 14.
Defant, A. 1961 *Physical Oceanography*, 2 vols. Pergamon.
Duncan, I. B. 1966 *J. Fluid Mech.* **24**, 417.
Eckhaus, W. & de Jager, E. M. 1966 *Arch. rat. Mech. Anal.* **23**, 26.
Elder, J. W. 1968 To be published.

ERDÉLYI, A. (Ed.) 1953 *Higher Transcendental Functions.* McGraw–Hill.

GOLDSTEIN, S. 1938 *Modern Developments in Fluid Dynamics.* Oxford.

GORDON, A. L. 1967 *Science,* **156,** 1732.

KAMENKOVICH, V. M. 1961 *Dokl. Akad. Nauk. SSSR,* **138,** 1076.

KAMENKOVICH, V. M. 1962 *Trudy Inst. Okeanol.* **56,** 241.

KORT, V. G. 1962 *Scient. Am.* **207,** 113.

LONGUET-HIGGINS, M. S. 1965 *Deep-Sea Res.* **12,** 923.

MCKEE, W. D. 1966 Survey Paper 1, Horace Lamb Centre for Oceanographical Research, Flinders University of South Australia.

STOMMEL, H. 1948 *Trans. Am. geophys. Un.* **29,** 202.

STOMMEL, H. 1957 *Deep-Sea Res.* **4,** 149.

STOMMEL, H. 1962 *J. mar. Res.* **20,** 92.

SVERDRUP, H. U. 1947 *Proc. natn. Acad. Sci. U.S.A.* **33,** 318.

WYRTKI, K. 1960 *Dt. hydrog. Z.* **13,** 153.